Infrared reflectance, transmittance, and emittance spectra of MgO from first principles

Giorgia Fugallo and Benoit Rousseau
CNRS, UMR 6607, Laboratoire de Thermique et Energie de Nantes, Polytech Nantes, Université de Nantes,
Rue Christian Pauc, F-44306 Nantes Cedex 3, France

Michele Lazzeri
Sorbonne Université, MNHN, IRD, CNRS UMR 7590, Institut de Minéralogie, de Physique des Matériaux et de Cosmochimie,
4 place Jussieu, F-75005 Paris, France

(Received 12 October 2018; published 28 November 2018)

By using density functional theory calculations we determined the influence of anharmonic effects on the infrared reflectance, transmittance, and emittance of MgO. The goal is to determine the limit of validity of a perturbative (multiphonon) approach. MgO is chosen as a test material because of the availability of different kinds of radiative properties measured experimentally. Nonanalytic terms of the three-phonon scattering coefficients are explicitly calculated and do not provide measurable effects. The agreement is overall very good to such an extent that, already at room temperature, one can clearly identify regions in which four-phonon scattering processes are dominant with respect to the three-phonon ones. The influence of isotopic disorder at cryogenic temperatures is also settled.

DOI: 10.1103/PhysRevB.98.184307

I. INTRODUCTION

Density functional theory (DFT) is considered a predictive approach to determine anharmonic phonon-phonon interactions in crystals [1]. Such a computational tool is a necessary ingredient, for example, of the first-principles computational methods recently developed to evaluate phonon thermal transport in real systems [2–9]. In this context, finding measurable quantities that can provide an independent benchmark for theoretical approaches is of paramount importance. Surprisingly, DFT has rarely been used to interpret the anharmonic features observable in IR reflectance, transmittance, and emittance spectra. These kind of spectra provide a relatively direct probe to anharmonic properties in heteropolar materials and can be used to directly determine the anharmonic phonon self-energy of the optically active modes [10,11].

In addition, the ability to simulate anharmonic properties of the dielectric constant is expected to have an impact on radiative heat-transfer studies [12]. For homogeneous heteropolar compounds (single crystals, glass), the key quantity for describing the ensemble of radiative exchanges is the spectral emittance for a range of wave numbers from 200 to 1500 cm^{-1}. This adimensional quantity is defined as the ratio of the spectral emissive power of a body to the spectral emissive power of the blackbody at the same temperature. Modeling an appropriate dielectric response allows us to determine microscopic mechanisms responsible for the macroscopic radiative behavior. Improving our knowledge of radiative heat exchanges could have practical aspects for the elaboration of new materials working at high temperatures (refractory materials for solar-to-heat conversion, nuclear reactor cores, thermal shields for space shuttles, infrared emitters) or for temperature measurements in extreme conditions via contactless methods (pyrometry, IR thermography).

MgO is very well characterized experimentally, and it is also a system of choice for DFT calculations given the excellent agreement with measured phonon dispersions [13]. But a close look at the literature reveals that several questions are still open. Indeed, Ref. [14] shows that reflectance- and transmittance-measured spectra can be used to determine the phonon self-energy in a wide spectral range ($0 < \omega < 2000\ \mathrm{cm}^{-1}$). However, in that work, the phonon self-energy is determined after a fitting procedure limiting the physical interpretation and not allowing predictions for materials whose spectra are not known. Reference [15] reports reflectivity measurements and shell-model calculations for $\mathrm{Mg}_{1-x}\mathrm{Fe}_x\mathrm{O}$, showing that the relevant characteristics of the spectra are well captured by three-phonon anharmonic scattering. From the measurements of Ref. [15] one can, however, extract relevant information only in a limited frequency range (i.e., for $\omega < 800\ \mathrm{cm}^{-1}$, within the reststrahlen band). References [16,17] reported first-principles molecular-dynamics (MD) calculations which can be used to interpret reflectivity in a wide temperature range. Unfortunately, the results that can be obtained by MD are not as detailed as those that can be obtained with a phonon-scattering perturbative approach (as in Ref. [15]). More recently, Ref. [18] reported DFT calculations of the three-phonon relaxation of the IR-active MgO optical phonon to study dielectric-loss measurements in a low-frequency spectral range ($<200\ \mathrm{cm}^{-1}$). The results of Ref. [18] include only coalescence three-phonon scattering processes and are not useful above 200 cm^{-1}, where decay scattering processes dominate.

Another question that needs to be addressed concerns the role of the so-called nonanalytic terms in the phonon-phonon scattering. Although these terms are usually assumed to be negligible, a few examples of this kind of study are actually present in the literature [19]. A direct evaluation for MgO is then desirable.

In the present work, to clarify the situation we calculate the influence of anharmonic effects, including both three- and four-phonon scattering processes, on the infrared reflectance, transmittance, and emittance spectra of rocksalt MgO by using DFT. The goal is to determine the limit of validity of a perturbative (multiphonon) approach.

II. GENERAL CONSIDERATIONS

Given an electromagnetic wave incident on the flat surface of a material, reflectance R and transmittance $\mathcal{T}$ are the fraction of the reflected and transmitted power. At the local thermal equilibrium and by considering Kirchoff's law of thermal radiation, the emittance can then be defined as $E = 1 - R - \mathcal{T}$. For a slab of finite thickness, R and $\mathcal{T}$ can be obtained once the complex dielectric function $\tilde{\epsilon}(\omega)$ of the material is known. Here, ω is the frequency of the light and, for simplicity, we consider an isotropic crystal ($\tilde{\epsilon}$ is then a scalar). R and $\mathcal{T}$ include the effects of multiple reflections between the two faces of the slab. Let us call r the reflectivity (which is the reflectance of a semi-infinite slab) and τ the power-loss factor. In the case of normal incidence, by solving the Maxwell equations [14,20],

$$r = \left|\frac{\sqrt{\tilde{\epsilon}} - 1}{\sqrt{\tilde{\epsilon}} + 1}\right|^2, \quad \tau = \exp[-4\pi d \mathrm{Im}(\sqrt{\tilde{\epsilon}})/\lambda],$$

$$\mathcal{T} = \frac{\tau(1-r)^2}{1 - r^2\tau^2}, \quad R = r(1 + \tau\mathcal{T}), \quad E = 1 - R - \mathcal{T}. \tag{1}$$

Here, the quantities $\tilde{\epsilon}$, r, τ, R, and $\mathcal{T}$ are functions of ω. d is the thickness of the slab, $\mathrm{Im}(z)$ is the imaginary part of the complex number z, and $1/\lambda = \omega/(2\pi c)$ is the wave number.

Let us consider a heteropolar crystal with only one optical phonon mode (the generalization is straightforward). According to the Lorentz model,

$$\tilde{\epsilon}(\omega) = \epsilon_\infty + \frac{S\omega_0^2}{\omega_0^2 - \omega^2 - i\omega\gamma}, \tag{2}$$

where ϵ_∞ is the electronic dielectric constant and ω_0, S, and γ are the frequency, oscillator strength, and damping (FWHM) of the TO phonon mode. Using the notation of Ref. [1], $S = 4\pi Z^2/(v\mu\omega_0^2)$, where Z is the Born effective charge, μ is the reduced mass of the oscillator, and v is the unit-cell volume of the crystal. A classical result of solid-state physics is that Eq. (2) explains the presence of the so-called reststrahlen band in the infrared reflectivity of heteropolar crystals. Equation (2) does not, however, explain the additional features observed within the reststrahlen band (see, e.g., Fig. 6.32 of Ref. [21]) in simple crystals.

A more general form for $\tilde{\epsilon}(\omega)$ can be obtained within perturbation theory [10,11],

$$\tilde{\epsilon}(\omega) = \epsilon_\infty + \frac{S\omega_0^2}{\omega_0^2 - \omega^2 + 2\omega_0\Pi(\omega)}, \tag{3}$$

where $\Pi(\omega)$ is the frequency-dependent self-energy of the TO phonon, accounting for anharmonic phonon-phonon interactions. $\Pi(\omega)$ is a complex quantity which can be decomposed as $\Pi(\omega) = \Delta(\omega) - i\Gamma(\omega)$ (with Δ and Γ being real). While $\Delta(\omega_0)$ is the anharmonic shift of the TO phonon frequency, $\Gamma(\omega_0)$ is its anharmonic broadening (half width at half maximum (HWHM); see, e.g., [22,23]). The most important difference between Eqs. (2) and (3) is that, while in Eq. (2) the damping is a constant, in Eq. (3) it depends on ω (by comparing Eqs. (2) and (3) the frequency-dependent damping is actually $\gamma(\omega) = 2\omega_0\Gamma(\omega)/\omega$; see Ref. [24]). This can have observable consequences when $\Gamma(\omega)$ displays sudden variations.

The physical meaning of the frequency-dependent broadening is not obscure. Equations (2) and (3) represent the response to an electromagnetic field oscillating with frequency ω, and thus, the polar atoms are forced to oscillate at ω. Moreover, the anharmonic broadening is given by a sum of scattering processes in which the energy is conserved [10,22,23], but the energy of the initial vibration is ω and not ω_0 (the frequency of the decoupled TO mode). $\Gamma(\omega)$ is actually expected to undergo sudden variations [14] since the possibility to decay in certain phonon branches becomes available only below certain energy thresholds (because of the energy conservation). This is especially true for simple crystals (a few atoms per unit cell) where Van Hove singularities in the phonon density of state are, generally, more pronounced.

III. COMPUTATIONAL APPROACH

In the present work, we consider the phonon self-energy Π to be the sum of the following contributions:

$$\Pi(\omega) = \Pi^{(3ph)}(\omega) + \Pi^{(4ph)}(\omega) + \Pi^{(isot)}(\omega), \tag{4}$$

$$\Pi^{(3ph)}(\omega) = \Pi^{(B)}(\omega) + \Pi^{(L)} + \Delta\omega^a. \tag{5}$$

$\Pi^{(3ph)}$ and $\Pi^{(4ph)}$ are the contributions whose imaginary part is due to three- and four-phonon anharmonic scatterings, respectively. $\Pi^{(isot)}$ is the self-energy component due to isotopic-disorder scattering.

$\Pi^{(B)}(\omega)$ and $\Pi^{(L)}$ are defined in Ref. [23] (see also [22]). $\Delta\omega^a$ corresponds to the optical-mode harmonic-frequency shift associated with the lattice thermal expansion. $\Pi^{(L)}$ and $\Delta\omega^a$ are not actually due to three-phonon scattering, but they are real and do not depend on ω. $\Pi^{(B)}(\omega)$ is due to three-phonon scattering, has an imaginary component, and depends on ω. $\Pi^{(B)}(\omega)$, $\Pi^{(L)}$, and $\Delta\omega^a$ are gathered together into $\Pi^{(3ph)}$ because they are the lowest-order terms in the perturbative expansion, $\Pi = \Pi^{(3ph)} + O(\hbar^2)$ [22,23], and thus, they are expected to provide a shift of the same order of magnitude. We remark, however, that the important characteristics of the spectra presently shown are determined by the imaginary part of $\Pi(\omega)$. The real part provides contributions negligible on the scale of the figures. The only notable exception concerns the position of the rise of the reststrahlen band near ω_0, which is sensitive to this frequency shift.

$\Pi^{(4ph)}(\omega)$ is the four-phonon scattering contribution corresponding to Eq. (2.15b) of Ref. [25]. It is imaginary and frequency dependent. The corresponding real part (Eq. (2.14c) of [25]) is included but does not provide relevant changes to the figures. Finally, the isotopic-disorder contribution $\Pi^{(isot)}(\omega)$ is calculated using Eq. (11) of Ref. [26], noting that $1/\tau$ in Ref. [26] is the FWHM, while with the present definitions Γ corresponds to HWHM. The needed mass variances are determined using data from Ref. [27].

All the described quantities can be calculated entirely from first principles with the method of Ref. [1]. DFT calculations were done with the QUANTUM ESPRESSO package [28] within the pseudopotential [29] and the local-density approximation [30] (LDA; 100 Ry plane-wave cutoff and $3 \times 3 \times 3$ shifted electronic integration grid). These approximations (DFT+LDA) are chosen since they are known to reproduce MgO phonon dispersion extremely well [13,18]. Reflectance and transmittance spectra are tremendously sensitive to LO and TO phonon mode dispersion, so that this extremely good agreement is a *conditio sine qua non* to well describe all the features of these spectra. The calculation of certain terms of Π is not trivial since one needs to determine the anharmonic phonon-scattering coefficients (APSCs) among all the possibly involved phonons. $\Pi^{(B)}$ depends on three-phonon scattering, and the APSCs among three phonons with distinct wave vectors can be calculated with the approach of [31,32]. To calculate $\Pi^{(L)}$ and $\Pi^{(4ph)}$ one needs to determine scattering among four distinct phonon modes. However, since one of the phonons is the optical mode at zero wave vector, $\mathbf{q} = 0$, the needed APSC can be determined by finite-difference differentiation (displacing the atoms along the $\mathbf{q} = 0$ optical mode) of a three-phonon APSC calculated as in [32]. All the scatterings were first calculated on a $4 \times 4 \times 4$ phonon wave vector grid and then Fourier interpolated on a $100 \times 100 \times 100$ grid (the procedure is described in detail in Ref. [32]). Tests were done using up to $8 \times 8 \times 8$ grids. The equilibrium lattice spacing of MgO is $a_0 = 4.198$ Å, corresponding to $\omega_0 = 411.8\ \mathrm{cm}^{-1}$. To determine $\Delta\omega^a$ we need to determine the dependence of the lattice spacing on the temperature $a(T)$. Here, $a(T)$ can be calculated using the quasiharmonic approximation [13], which, however, for MgO, overestimates the thermal expansion above $T = 295$ K [13]. We then used quasiharmonic calculations to determine the $T = 0$ lattice spacing $a(0)$, which turns out to be 0.43% higher than a_0 [$a(0) \neq a_0$ because of zero-point motion], compatible with calculations in Ref. [13]. For a given temperature, we then considered the measured relative lattice thermal expansion, taken from Ref. [33], to determine $a(T)$. By calculating the harmonic frequency of the TO mode at the lattice spacings thus obtained, we have $\Delta\omega^a = -12.3, -16.6, -41\ \mathrm{cm}^{-1}$ for $T = 0$, 295, 950 K, respectively. At the same temperatures the shift associated with $\Pi^{(L)}$ is $+9.5, +12.7, +32\ \mathrm{cm}^{-1}$, and that from $\Pi^{(B)}(\omega_0)$ is $-6.1, -8.7, -22\ \mathrm{cm}^{-1}$. The total anharmonic shift of ω_0 is then $-8.9, -12.6, -31\ \mathrm{cm}^{-1}$ at $T = 0$, 295, 950 K, respectively. Determining the shift in this way for higher temperatures would be misleading since higher-order terms should be relevant.

Finally, from the present DFT calculations $\epsilon_\infty = 3.10$ [which should be used in Eq. (3)]. This value slightly overestimates the experimental value $\epsilon_\infty = 2.94$ because of a well-known error of DFT [34]. Unless otherwise stated, in the following we will use $\epsilon_\infty = 2.94$. This is the only fitted parameter of the simulations and allows a better description of the high-energy reflectance and of the LO frequency drop of the reststrahlen band.

IV. NONANALYTIC TERM CONTRIBUTION

In insulating heteropolar materials the dynamical matrix can be decomposed in two components with or without an analytic dependence on the wave vector $\mathbf{q}$ [1]. The nonanalytic component is determined by the Born effective charges and is associated with the LO/TO splitting phenomenon. A similar analytic/nonanalytic decomposition can be done for the anharmonic phonon-phonon scattering coefficients necessary to compute the phonon self-energy (see, e.g., Ref. [19]). In a different point of view, following Cowley's work [10], there are six contributions to the susceptibility, associated with the six diagrams from Fig. 10 of Ref. [10]. These contributions are of the same order in $\hbar$, but while the first one (the most commonly used and described in the literature) depends only on the first derivative of the polarization with respect to atomic displacements, the others depend on higher-order derivatives. The calculations described in the previous sections include only analytic contributions, or, in other words, only the first of Cowley's diagrams.

The contributions from the other diagrams depend on the second derivative of the polarization and have been calculated by using finite differences of the Born effective charges calculated in a supercell (see Appendix A). It is interesting to notice that, by using an approach different from that described in Ref. [10], the inclusions of these diagrams can be done through an appropriate "dressing" of the phonon self-energy (see Appendix A), without modifying the usual expression for the dielectric constant [Eq. (3)]. This approach has the advantage of making transparent the link between Ref. [19], which provides two distinct expressions for the broadening of the TO and LO optical phonons, and Ref. [10], where the broadening of the LO phonon is not explicitly deduced. However, the correction of the self-energy associated with these diagrams is very small (see Appendix A) and, for the present purpose, can be neglected.

Cowley also described diagrams depending on the third derivative of the polarization (with respect to atomic positions), but according to direct calculations (see Appendix B), their contribution is also negligible: ~0.05% variation of Z at room temperature.

The calculations described in the present section and in the appendixes are corrections to the $\Pi^{(3ph)}$ term in Eq. (4). Given their negligible impact, one can safely assume that analogous corrections for the $\Pi^{(4ph)}$ term should not be relevant.

V. RESULTS AND DISCUSSION

Figures 1(a) and 1(b) compare different kinds of calculations with the room-temperature reflectance and transmittance measurements from Ref. [14]. Calculations labeled L′ and L are done by considering a frequency-independent self-energy, $\Pi(\omega) = \Pi(\omega_0)$, and thus correspond to the Lorentz model, Eq. (2). As expected [14], this kind of approach reproduces measurements only at a qualitative level. All the parameters used for the L′ model are from DFT calculations; in particular L′ is done by using $\epsilon_\infty = 3.10$. The only difference between

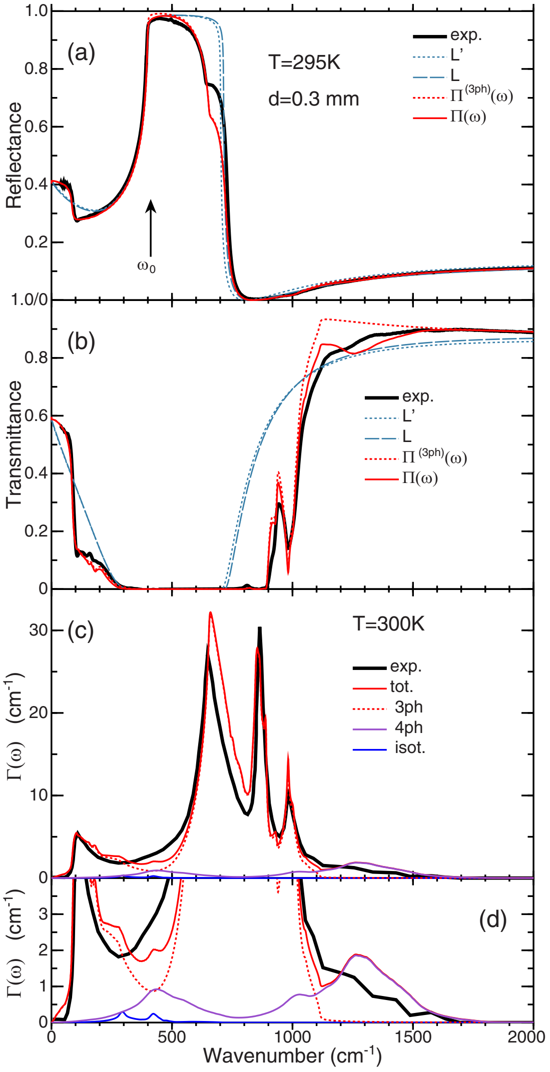

FIG. 1. (a) and (b) MgO infrared room-temperature reflectance and transmittance for a $d = 0.3$ mm thick plate. Measurements (exp.) are from Ref. [14]. All the other lines are calculations done at the different levels of approximation described in the text. $\Pi(\omega)$ represents our best result. The vertical arrow indicates the harmonic TO phonon frequency. (c) and (d) $\Gamma(\omega) = -\text{Im}[\Pi(\omega)]$, where Π is the calculated self-energy of the TO mode, Eq. (4). Data taken from Ref. [14] (exp.) vs the present calculation (tot.) decomposed into three-phonon (3ph), four-phonon (4ph), and isotopic-disorder (isot.) contributions. (c) and (d) report the same data on different scales.

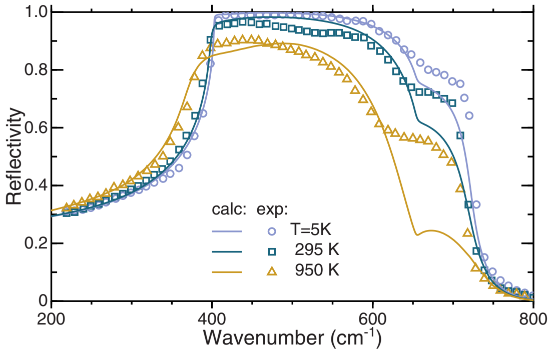

FIG. 2. IR reflectivity at various temperatures: calculations (calc.) vs measurements (exp.) from Ref. [35].

the L′ and L models is that, in the last case, for ϵ_∞ in Eq. (3) we have used the experimental value $\epsilon_\infty = 2.94$ [34]. The comparison between L′ and L calculations from Fig. 1(a) illustrates the influence of this parameter. In particular, by using the ϵ_∞ experimental value (L model), one obtains a better calculation/measurement agreement for ω_0 (related to the reflectance drop position of the reststrahlen band) and for the high-frequency ($\omega > 1000$ cm^{-1}) behavior of the reflectance.

In Figs. 1(a) and 1(b), calculations labeled $\Pi^{(3ph)}$ include only the lowest-order terms of the self-energy [$\Pi^{(4ph)} = \Pi^{(isot)} = 0$ in Eq. (4)], while Π labels our best calculations including all the terms in Eq. (4). From Fig. 1(a), the inclusion of the lowest-order terms in the self-energy $\Pi^{(3ph)}$ reproduces very well the reflectance in the low-frequency region, $\omega < 150$ cm^{-1}, and the position of the shoulder observed at $\sim$650 cm^{-1} within the reststrahlen band. The inclusion of four-phonon and isotopic scatterings provides only a small but observable improvement in the 400/500 cm^{-1} region.

From Fig. 1(b), the measured transmittance is also very well reproduced. Here, however, the lowest-order processes $\Pi^{(3ph)}(\omega)$ are not able to reproduce data above 1100 cm^{-1}. Indeed, above $\sim$1100 cm^{-1} three-phonon decay processes go to zero because of the unavailability of scattering channels, and only the inclusion of four-phonon processes [included in $\Pi(\omega)$] can provide a reasonable agreement with measurements.

Figures 1(c) and 1(d) show the imaginary part of the self-energy $\Gamma(\omega)$ and compare it with that taken from Ref. [14] (see Fig. 3 of Ref. [15] for an analogous comparison with the shell-model calculation). We recall that the $\Gamma(\omega)$ from Ref. [14] is an arbitrary-shape function inserted into the dielectric function expression in order to fit the experimental spectra. Having this in mind and considering that the authors of Ref. [14] did not have access to an independent determination of $\Gamma(\omega)$, the agreement with the present calculation is remarkable: the presence of four major peaks at $\sim$105, 650, 860, and 990 cm^{-1} and their shape are indeed consistently described by the two approaches. Note that the three-phonon contribution to Γ has a minimum near 400 cm^{-1}. This energy separates remarkably well a low-frequency region where three-phonon coalescence processes are dominant (at room temperature) with respect to decay ones from a high-frequency region where decay processes are dominant.

The most evident disagreement in Fig. 1(c) concerns the intensity of the 650-cm^{-1} peak, which determines the presence of the reflectance shoulder at that frequency. DFT-LDA calculations overestimate the intensity of this peak by $\sim$30%, and this disagreement cannot be attributed to the neglect of some terms in the calculations (which would eventually further increase the peak). This problem is observable already at cryogenic temperatures and becomes more evident by increasing the temperature, as can be seen in the reflectivity spectra in Fig. 2. Indeed, already at $T = 5$ K, the intensity of the calculated reflectivity shoulder (at $\sim$650 cm^{-1}) clearly underestimates the measurements.

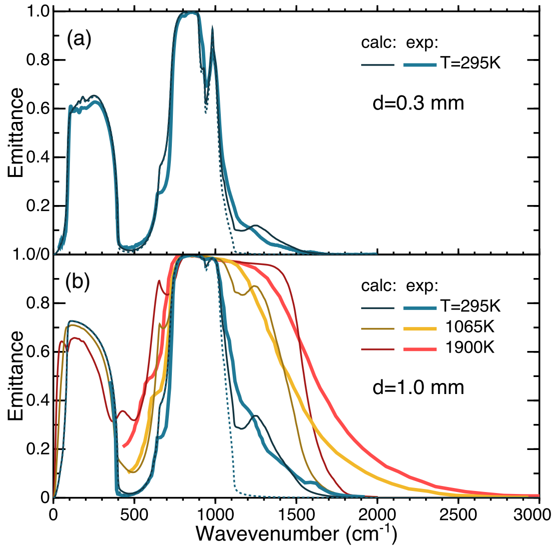

FIG. 3. IR emittance at various temperatures: calculations (calc.) vs measurements (exp.). (a) Measurements from Ref. [14] (the same as in Fig. 1) and (b) measurements digitized from Ref. [36]. Here, d is the thickness of the plate. Dotted lines are $T = 295$ K calculations including only three-phonon scattering (and not four-phonon ones).

Let us go back to Figs. 1(c) and 1(d). The four-phonon scattering contribution to $\Gamma(\omega)$ is visible in two regions: above 1100 cm^{-1}, where it is the dominant contribution, and in the 300/500 cm^{-1} region. Here, the three-phonon scattering is relatively small and becomes comparable to both four-phonon and isotopic-disorder contributions. The importance of the four-phonon contribution in the high-frequency domain is evident in the emittance spectra of Fig. 3. Already at room temperature ($T = 295$ K $\sim 0.1T_\mathrm{m}$, where T_m is the melting temperature) there is an evident disagreement between measurements and calculations done including only three-phonon scattering. At $T = 295$ K, the inclusion of four-phonon processes is, however, enough to have reasonable agreement in the whole spectral range [Figs. 3(a) and 3(b)]. This approach still provides qualitative agreement in a relatively wide spectral range (up to 1500 cm^{-1}) at high temperatures [$T =$ 1065 K $\sim 0.3T_\mathrm{m}$; Fig. 3(b)].

At room temperature, the broadening due to isotopic disorder is, overall, negligible. However, this contribution does not depend on temperature and is present in a region in which Γ is relatively small [Figs. 1(c) and 1(d)]. Because of this, it becomes very visible at cryogenic temperatures in the transmittance spectra. Indeed, Fig. 4 compares the present calculations with the transmittance measurements from Ref. [37]. The agreement for temperatures below 100 K is extremely good and clearly indicates that the measured "valley" at $\sim$300 cm^{-1} is due to isotopic disorder.

Finally, to make a comparison with similar data available in the literature [14,35], Fig. 5 reports the imaginary part of the dielectric function and the extinction coefficient, calculated at various temperatures. Calculations above $T = 295$ K cannot be considered quantitatively correct but are given as a reference. On the other hand, Fig. 6 reports emissivity spectra (defined as $1 - \tau$) calculated for various values of the thickness parameter d and compared with those obtained in Ref. [38]. Data from Ref. [38] were obtained from classical dispersion analysis [39], using parameters obtained after fitting of reflectivity measurement (for $0.1 \leqslant d \leqslant 5$ μm) or derived from the measured absorbance (for $10 \leqslant d \leqslant 100$ μm). The procedure of Ref. [38] captures the overall behavior of the emissivity, which for small d mimics absorption spectra with a prevalent strong peak around 400 cm^{-1}, while for larger d values becomes pinned at unity in the absorbing region. However, the comparison of Figs. 6(a) and 6(b) confirms how fitting reflectance measurements provides a limited amount of information in the low-frequency region ($\omega < 200$ cm^{-1}) and misses important features above 700 cm^{-1}, where anharmonicity becomes relevant. In this region, data derived from absorbance measurements [$d \geqslant 10\,\mu$m in Fig. 6(b)] provide a reasonable description of the emissivity but were not used to describe the low-frequency behavior. Calculations in Fig. 6(a) are done at room temperature to compare them with those in Ref. [38]. Higher temperatures would cause additional broadening, whereas cryogenic features would be narrower [38].

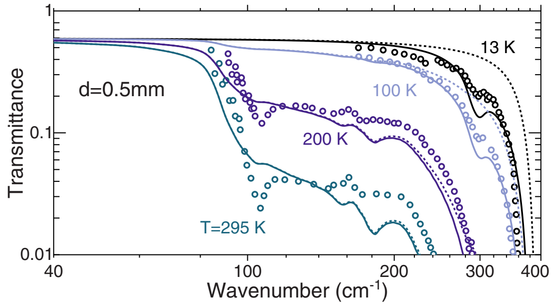

FIG. 4. Temperature evolution of the MgO transmittance for a 0.5-mm-thick plate. Dots are measurements digitalized from [37]. Dotted lines are calculations in which the isotopic-disorder contribution is set to zero. Solid lines are our best calculations (which include isotopic disorder).

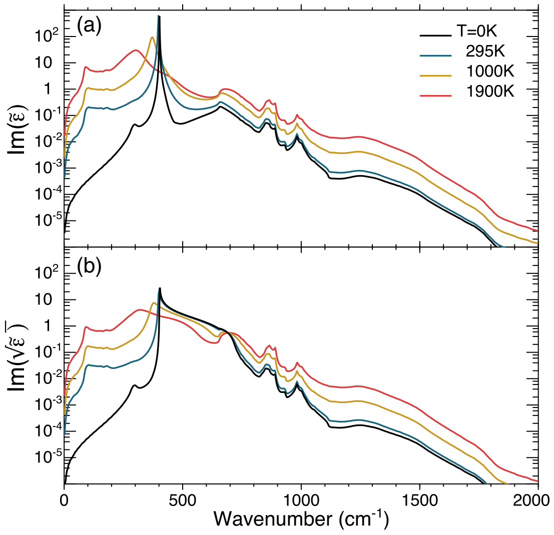

FIG. 5. Calculated imaginary part of the dielectric constants and extinction coefficient at various temperatures.

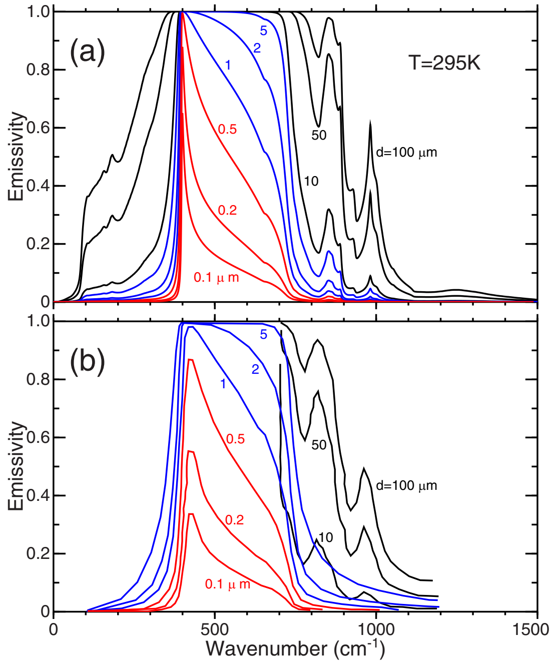

FIG. 6. Room-temperature emissivity (defined as $1-\tau$) calculated for various thicknesses d. (a) Present calculations. (b) Data digitalized from Ref. [38] (see the text).

VI. CONCLUSIONS

We studied anharmonic (multiphonon) features of the infrared spectra of MgO using first-principles (DFT) calculations. Nonanalytic terms of the three-phonon scattering coefficients were explicitly calculated and do not provide measurable effects. Concerning reflectivity, which probes a limited frequency range, the frequency of the most relevant spectral features is well described by DFT, and only the intensity of the intense peak of the phonon self-energy at $\sim$640 cm^{-1} is overestimated. On the other hand, by comparing calculations with transmittance and emittance data (which probe a much wider range), the agreement is, overall, very good, to the extent that, already at room temperature, one can clearly identify regions in which four-phonon scattering is dominant with respect to the three-phonon one. The influence of isotopic disorder (negligible at room temperature) is evident at cryogenic temperatures.

ACKNOWLEDGMENTS

M.L. thanks Ch. Brouder and E. Balan for useful discussions. Calculations were performed at IDRIS (Orsay) within Project No. 100834.

APPENDIX A: LO SELF-ENERGY DRESSING

According to Cowley's work [10], at the lowest order, there are six contributions to the susceptibility, associated with the six diagrams [labeled (a)–(f)] from Fig. 10 of Ref. [10]. The first contribution, (a), is the most commonly described/used in the literature, and it is included in the approach described in Sec. III. Here, we describe how contributions (b)–(d) have been calculated. Appendix B will then report on the calculation of diagrams (e) and (f).

Let us consider a crystal and call u_{ls} the displacement of one atom in the unit cell identified by the lattice vector $\mathbf{R}_l$. The index s defines the atom in the unit cell and the Cartesian coordinate. $\omega_{\mathbf{q}j}$ and $z_s^{\mathbf{q}j}$ are the angular frequency and the eigenvector (orthonormal in the unit cell) of the phonon with wave vector $\mathbf{q}$ and branch index j. The Born effective charges can be defined as $Z_s^{\alpha} = \frac{1}{N}\sum_l \frac{\partial M^{\alpha}}{\partial u_{ls}}$, where M^{α} is the total polarization of the crystal along the Cartesian coordinate α and N is the number of cells. The charge associated with a specific $\mathbf{q}=0$ mode can then be defined as

$$M^{\alpha}_{\mathbf{0}j} = \sum_s \sqrt{\frac{\hbar}{2m_s\omega_{\mathbf{0}j}}}\, z_s^{\mathbf{0}j} Z_s^{\alpha}, \qquad \text{(A1)}$$

where m_s is the mass of the atom associated with the s index. Z_s^{α} and $M^{\alpha}_{\mathbf{0}j}$ can be routinely calculated thanks to the computational approach described in Ref. [1]. We now define

$$M^{\alpha}_{-\mathbf{q}j,\mathbf{q}j'} = \frac{1}{N}\sum_{l,l',s,s'} \sqrt{\frac{\hbar}{2m_s\omega_{\mathbf{q}j}}}\sqrt{\frac{\hbar}{2m_{s'}\omega_{\mathbf{q}j'}}}\, z_s^{-\mathbf{q}j} z_{s'}^{\mathbf{q}j'} \times e^{i\mathbf{q}\cdot(\mathbf{R}_{l'}-\mathbf{R}_l)} \frac{\partial^2 M^{\alpha}}{\partial u_{ls}\partial u_{l's'}}. \qquad \text{(A2)}$$

This quantity is a necessary ingredient to calculate Eqs. (6.9) and (6.10) of Ref. [10], corresponding to Cowley's diagrams (b)–(d). In the present work, the second derivative of the polarization with respect to atomic displacements has been calculated on a $3\times3\times3$ MgO supercell by finite differentiation of the Born effective charges with respect to finite displacements of the atomic positions. $M^{\alpha}_{-\mathbf{q}j,\mathbf{q}j'}$ can then be determined at any $\mathbf{q}$ by standard Fourier interpolation techniques. Analogous calculations have been reported, for example, in Ref. [19] to determine the broadening of the LO optical phonon and in Refs. [40,41] to determine the two-phonon spectrum of Si and Ge.

To study the effects of this interaction, let us consider the dielectric tensor is $\tilde{\epsilon}^{\alpha,\beta}(\omega) = \epsilon_{\infty}^{\alpha,\beta} + 4\pi\chi^{\alpha,\beta}(\omega)$, with

$$\chi^{\alpha,\beta}(\omega) = \frac{1}{v\hbar}\sum_j \frac{2\omega_{\mathbf{0}j} M^{\alpha}_{\mathbf{0}j} M^{\beta}_{\mathbf{0}j}}{\omega^2_{\mathbf{0}j} - \omega^2 - 2\omega_{\mathbf{0}j}\Pi_{\mathbf{0}j}(\omega)}. \qquad \text{(A3)}$$

Here, v is the unit-cell volume, and the sum runs over the optical modes with $\mathbf{q}=0$. In the present case the optical modes number three, are degenerate, and can be considered polarized along the three Cartesian directions. The expression can then be simplified with

$$\chi^{\alpha,\beta}(\omega) = \frac{1}{v\hbar}\frac{2\omega_0 M_0^2}{\omega_0^2 - \omega^2 + 2\omega_0\Pi_{\alpha}(\omega)}\delta_{\alpha,\beta}, \qquad \text{(A4)}$$

where $M^{\alpha}_{\mathbf{0}\beta} = \delta_{\alpha,\beta}M_0$ and $\omega_{\mathbf{0}\beta} = \omega_0$. To further simplify the discussion, we consider only the $\Pi^{(B)}(\omega)$ contribution from Eq. (5), having

$$\Pi_{\alpha}(\omega) = \frac{-1}{N\hbar^2}\sum_{\mathbf{q},j,j'} \left|V^{(3)}_{\mathbf{0}\alpha,-\mathbf{q}j,\mathbf{q}j'}\right|^2 F(\omega,\omega_{\mathbf{q}j},\omega_{\mathbf{q}j'}). \qquad \text{(A5)}$$

Here, the three-phonon scattering coefficients $V^{(3)}$ are defined as in Ref. [32], Π_{α} does not depend on the α direction because

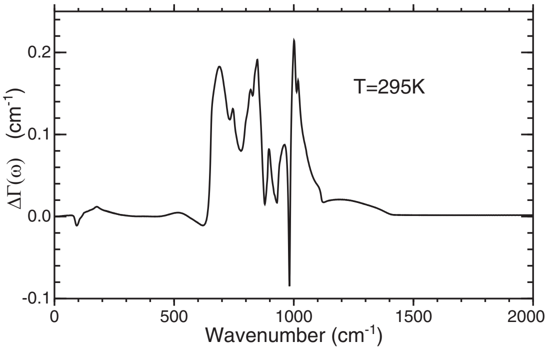

FIG. 7. Self-energy of the $\mathbf{q} = 0$ optical phonon of MgO at room temperature: variation of the imaginary part after the inclusion of the nonanalytic corrections to the three-phonon scattering. $\Delta\Gamma(\omega)$ is defined in the text.

of symmetry, and

$$F(\omega,\omega_1,\omega_2) = \frac{(1+n_1+n_2)(\omega_1+\omega_2)}{(\omega_1+\omega_2)^2-(\omega+i\eta)^2} + \frac{(n_2-n_1)(\omega_1-\omega_2)}{(\omega_1-\omega_2)^2-(\omega+i\eta)^2}, \tag{A6}$$

where n_1 and n_2 are the temperature-dependent Bose-Einstein occupations related to ω_1 and ω_2.

After some algebra, one can see that the inclusion of Cowley's diagrams (b)–(d), which can be calculated with Eqs. (6.8), (6.9), and (6.10) of Ref. [10], is equivalent (at the same order in $\hbar$) to substituting $V^{(3)}$ in Eq. (A5) with

$$\tilde{V}^{(3)}_{\mathbf{0}\alpha,-\mathbf{q}j,\mathbf{q}j'} = V^{(3)}_{\mathbf{0}\alpha,-\mathbf{q}j,\mathbf{q}j'} - \hbar\frac{M^{\alpha}_{-\mathbf{q}j,\mathbf{q}j'}}{M_0}\frac{\omega_0^2-\omega^2}{2\omega_0}. \tag{A7}$$

In practice, the effects of Cowley's diagrams (b)–(d) can be seen as a dressing of the three-phonon scattering. Note that Ref. [19] discusses only two special cases of Eq. (A7): $\omega = \omega_{\mathrm{TO}} = \omega_0$ and $\omega = \omega_{\mathrm{LO}}$. For $\omega = \omega_0$ (i.e., when the vibration is decoupled from the electric field oscillation) the dressing is zero. On the other hand, by inserting $\omega = \omega_{\mathrm{LO}}$ in Eq. (A7), after some algebra, one can obtain the expression for the broadening of the LO phonon already derived in Ref. [19] [keep in mind the comment on the damping given after Eq. (3) and that $\omega_{\mathrm{LO}}^2 - \omega_{\mathrm{TO}}^2 = 8\pi\omega_0 M_0^2/(\hbar v\epsilon_\infty)$].

Figure 7 shows the effects of correction of Eq. (A7) for the MgO $\mathbf{q} = 0$ optical mode. In particular, it reports $\Delta\Gamma(\omega) = \mathrm{Im}[\Pi(\omega) - \tilde{\Pi}(\omega)]$, where $\Pi(\omega)$ is obtained from Eq. (A5) as it is written and $\tilde{\Pi}(\omega)$ is obtained from Eq. (A5) by substituting $V^{(3)}$ with $\tilde{V}^{(3)}$ from Eq. (A7).

APPENDIX B: *Z* THERMAL AVERAGE

By looking at Eq. (6.11) of Ref. [10], it is easy to see that the inclusion of Cowley's diagrams (e) and (f) is equivalent to substituting $M^{\alpha}_{\mathbf{0}j}$ in Eq. (A3) with

$$\tilde{M}^{\alpha}_{\mathbf{0}j} = M^{\alpha}_{\mathbf{0}j} + \frac{1}{N}\sum_{\mathbf{q},j'} M^{\alpha}_{\mathbf{0}j,-\mathbf{q}j',\mathbf{q}j'} \times (2n_{\mathbf{q}j'}+1), \tag{B1}$$

where $M^{\alpha}_{\mathbf{0}j,-\mathbf{q}j',\mathbf{q}j'}$ can be defined by generalizing Eq. (A2) and $n_{\mathbf{q}j'}$ is the Bose-Einstein occupation associated with $\omega_{\mathbf{q}j'}$ for a temperature T. This kind of integral can be evaluated stochastically. Indeed, given a crystal and a generic quantity $F(\{u_{ls}\})$,

$$\langle F\rangle \simeq \frac{1}{N}\sum_{\mathbf{q}j} F_{-\mathbf{q}j,\mathbf{q}j}(2n_{\mathbf{q}}+1), \tag{B2}$$

where $\langle F\rangle$ is the quantum statistical average of F at the temperature T. $\langle F\rangle$ can be evaluated stochastically using the procedure described, e.g., in Ref. [42]. In practice, we considered a $3\times3\times3$ MgO supercell. We generated different configurations by displacing randomly the atomic positions as in Ref. [42] and averaged the resulting Born effective charges.

[1] S. Baroni, S. de Gironcoli, A. Dal Corso, and P. Giannozzi, Rev. Mod. Phys. **73**, 515 (2001).
[2] G. Fugallo, M. Lazzeri, L. Paulatto, and F. Mauri, Phys. Rev. B **88**, 045430 (2013).
[3] G. Fugallo, A. Cepellotti, L. Paulatto, M. Lazzeri, N. Marzari, and F. Mauri, Nano Lett. **14**, 6109 (2014).
[4] S. Lee, D. Broido, K. Esfarjani, and G. Chen, Nat. Commun. **6**, 6290 (2015).
[5] A. Cepellotti, G. Fugallo, L. Paulatto, M. Lazzeri, F. Mauri, and N. Marzari, Nat. Commun. **6**, 6400 (2015).
[6] T. Luo and G. Chen, Phys. Chem. Chem. Phys. **15**, 3389 (2013).
[7] L. Lindsay, D. A. Broido, and T. L. Reinecke, Phys. Rev. B **87**, 165201 (2013).
[8] L. Lindsay, Nanoscale Microscale Thermophys. Eng. **20**, 67 (2016).
[9] G. Fugallo and L. Colombo, Phys. Scr. **93**, 059501 (2018).
[10] R. A. Cowley, Adv. Phys. **12**, 421 (1963).
[11] F. Gervais, Mater. Sci. Eng. R **39**, 29 (2002).
[12] M. F. Modest, *Radiative Heat Transfer* (Academic, Oxford, 2013).
[13] B. B. Karki, R. M. Wentzcovitch, S. de Gironcoli, and S. Baroni, Phys. Rev. B **61**, 8793 (2000).
[14] D. De Sousa Meneses, J. Brun, P. Echegut, and P. Simon, Appl. Spectr. **58**, 969 (2004).
[15] T. Sun, P. B. Allen, D. G. Stahnke, S. D. Jacobsen, and C. C. Homes, Phys. Rev. B **77**, 134303 (2008).
[16] G. A. Adebayo, Y. Liang, C. R. Miranda, and S. Scandolo, J. Chem. Phys. **131**, 014506 (2009).
[17] J. Y. Yang, W. J. Zhang, L. H. Liu, J. Qiu, K. Wang, and J. Y. Tan, J. Chem. Phys. **141**, 104703 (2014).
[18] J. Breeze, *Temperature and Frequency Dependence of Complex Permittivity in Metal Oxide Dielectrics: Theory, Modelling and Measurement* (Springer, Berlin, 2016).
[19] G. Deinzer, M. Schmitt, A. P. Mayer, and D. Strauch, Phys. Rev. B **69**, 014304 (2004).
[20] J. D. Jackson, *Classical Electrodynamics* (Wiley, New York, 1998).
[21] Y. Yu and M. Cardona, *Fundamentals of Semiconductors*, 3rd ed. (Springer, Berlin, 2003).
[22] J. Menendez and M. Cardona, Phys. Rev. B **29**, 2051 (1984).

[23] M. Lazzeri, M. Calandra, and F. Mauri, Phys. Rev. B **68**, 220509(R) (2003).

[24] F. Gervais and B. Piriou, J. Phys. C **7**, 2374 (1974).

[25] M. Balkanski, R. F. Wallis, and E. Haro, Phys. Rev. B **28**, 1928 (1983).

[26] S. I. Tamura, Phys. Rev. B **27**, 858 (1983).

[27] J. S. Coursey, D. J. Schwab, J. J. Tsai, and R. A. Dragoset, (2015), Atomic Weights and Isotopic Compositions (version 4.1), National Institute of Standards and Technology, Gaithersburg, MD, http://physics.nist.gov/Comp.

[28] P. Giannozzi, O. Andreussi, T. Brumme, O. Bunau, M. Buongiorno Nardelli, M. Calandra, R. Car, C. Cavazzoni, D. Ceresoli, M. Cococcioni, N. Colonna, I. Carnimeo, A. Dal Corso, S. de Gironcoli, P. Delugas, R. DiStasio, A. Ferretti, A. Floris, G. Fratesi, G. Fugallo, R. Gebauer, U. Gerstmann, F. Giustino, T. Gorni, J. Jia, M. Kawamura, H. Y. Ko, A. Kokalj, E. Kücükbenli, M. Lazzeri, M. Marsili, N. Marzari, F. Mauri, N. L. Nguyen, H. V. Nguyen, A. Otero-de-la-Roza, L. Paulatto, S. Poncé, D. Rocca, R. Sabatini, B. Santra, M. Schlipf, A. P. Seitsonen, S. Smogunov, I. Timrov, T. Thonhauser, P. Umari, N. Vast, and S. Baroni, J. Phys.: Condens. Matter **29**, 465901 (2017).

[29] N. Troullier and J. L. Martins, Phys. Rev. B **43**, 1993 (1991).

[30] J. P. Perdew and A. Zunger, Phys. Rev. B **23**, 5048 (1981).

[31] M. Lazzeri and S. de Gironcoli, Phys. Rev. B **65**, 245402 (2002).

[32] L. Paulatto, F. Mauri, and M. Lazzeri, Phys. Rev. B **87**, 214303 (2013).

[33] Y. Sumino, O. L. Anderson, and I. Suzuki, Phys. Chem. Miner. **9**, 38 (1983).

[34] A. Schleife, C. Rödl, F. Fuchs, J. Furthmüller, and F. Bechstedt, Phys. Rev. B **80**, 035112 (2009).

[35] J. R. Jasperse, A. Kahan, and J. N. Plendl, Phys. Rev. **146**, 526 (1966).

[36] J. Brun, Ph.D. thesis, Université d'Orléans, 2003.

[37] G. A. Komandin, O. E. Porodinkov, I. E. Spector, and A. A. Volkov, Phys. Solid State **51**, 2045 (2009).

[38] A. M. Hofmeister, E. Keppel, and A. K. Speck, Mon. Not. R. Astron. Soc. **345**, 16 (2003).

[39] W. G. Spitzer, R. C. Miller, D. A. Kleinman, and L. W. Howarth, Phys. Rev. **126**, 1710 (1962).

[40] G. Deinzer and D. Strauch, Phys. Rev. B **69**, 045205 (2004).

[41] E. L. Shirley and H. M. Lawler, Phys. Rev. B **76**, 054116 (2007).

[42] R. Nemausat, C. Gervais, C. Brouder, N. Trcera, A. Bordage, C. Coelho-Diogo, P. Florian, A. Rakhmatullin, I. Errea, L. Paulatto, M. Lazzeri, and D. Cabaret, Phys. Chem. Chem. Phys. **19**, 6246 (2017).